Thiophene-Based Double Helices: Syntheses, X-ray Structures, and Chiroptical Properties

Sheng Zhang,[†] Xinming Liu,[‡] Chunli Li,[†] Lu Li,[†] Jinsheng Song,[*,†] Jianwu Shi,[†] Martha Morton,[‡] Suchada Rajca,[‡] Andrzej Rajca,[*,‡] and Hua Wang[*,†,§]
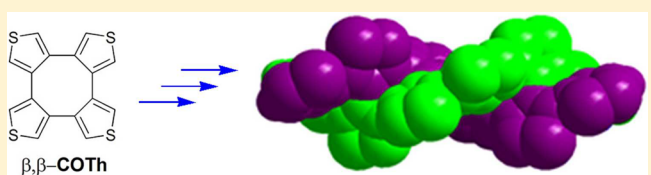
[†]Engineering Research Center for Nanomaterials, Henan University, Kaifeng 475004, China
[‡]Department of Chemistry, University of Nebraska, Lincoln, Nebraska 68588, United States
[§]Collaborative Innovation Center of Nano Functional Materials and Applications of Henan Province, Kaifeng 475004, China
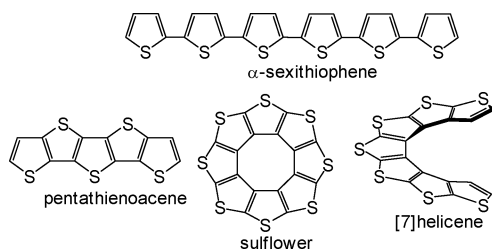
S *Supporting Information*

ABSTRACT: We demonstrate facile and efficient construction of conjugated double helical ladder oligomers from the saddle-shaped cyclooctatetrathiophene (**COTh**) building blocks. The key step involves deprotonation of tetra[3,4]-thienylene (β,β-**COTh**) with n-BuLi which displays remarkably high ipsilateral selectivity. Three racemic double helical ladder oligomers, *rac*-**DH-1**, *rac*-**DH-2**, and *rac*-**DH-3**, containing two, three, and five **COTh** annelated moieties are efficiently synthesized by diastereoselective coupling of the racemic precursors. The X-ray crystallographic studies of *rac*-**DH-1**, *rac*-**DH-2** and *rac*-**DH-3** unambiguously revealed that each double helical scaffold has two single helices intertwined with each other via the C—C single bonds. Following removal of TMS groups, double helical ladder oligomer *rac*-**DH-1-D** had sufficient solubility to be resolved via chiral HPLC, thus enabling determination of its chiroptical properties such as CD spectra and optical rotation. (+)-**DH-1-D** has a large barrier for racemization, with lower limit of $\Delta G^{\ddagger} > 48$ kcal mol^{-1}, which may be compared to DFT-computed barrier of 51 kcal mol^{-1}. The enantiomers of **DH-1-D** show 1 order of magnitude stronger chiroptical properties than the carbon—sulfur [7]helicene, as determined by the anisotropy factor $g = \Delta\varepsilon/\varepsilon = -0.039$, based on $\Delta\varepsilon_{max} = -11$ and $\varepsilon = 2.8 \times 10^2$ L mol^{-1} cm^{-1} in cyclohexane at 327 nm.

INTRODUCTION

Thiophene-based oligomers and polymers play a prominent role in the development of organic materials for technological applications.[1,2] The mainstream research has largely focused on linear α-oligothiophenes, such as α-sexithiophene, and their analogous fused thiophenes (thienoacene) oligomers, such as pentathienoacene (Figure 1).[1−3] Significant effort has been made in the design of highly annelated oligothiophenes that lead to novel zero- and one-dimensional (0-D and 1-D) carbon—sulfur molecules and oligomers. Among notable examples are sulflower (0-D)[4] and helical annelated β-oligothiophene, such as [7]helicene (1-D; Figure 1).[5,6] These novel structures have received considerable attention because

they are not only aesthetically pleasing but also have great potential in the design of organic functional materials with unique and tunable optical/electronic properties.[7]

We are motivated to explore the two-dimensional (2-D) carbon—sulfur structure. Alternating connectivity of the saddle-shaped tetraarylenes such as tetra[2,3]thienylene (α,β-cyclooctatetrathiophene, α,β-**COTh**) and tetra[3,4]thienylene (β,β-cyclooctatetrathiophene, β,β-**COTh**; Figure 2) may be conceived as composed of double helical polymers with alternating connectivity of α,β-**COTh** and β,β-**COTh**. Likewise, the all-thiophene double helices may be viewed as conjugated double helical ladder oligomers.[8] Such oligomers are of particular interest, due to their imaginative and extraordinary aesthetically pleasing structures with potential to possess very high racemization barriers, propensity for strong intermolecular interactions, and strong chiroptical properties.[9−12]

The double helical motifs connected by covalent bonds pertain to exotic macromolecules that are distinct from those noncovalently linked helices derived from supramolecular assembly of single strands by metal ion complexation,[13] aromatic interaction[14,15] and hydrogen bonding.[16,17] Design and synthesis of such macromolecules with double helical motif

**Figure 1.** Oligothiophenes and annelated carbon—sulfur molecules and oligomers.
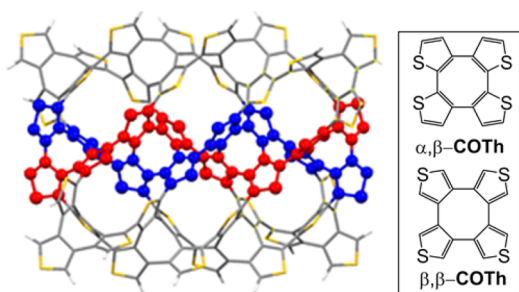
Figure 2. D_2-symmetric fragment of two-dimensional (2D) carbon–sulfur structure (geometry optimized at the AM1-level) and all-thiophene double helices with alternating connectivity of α,β-**COTh** and β,β-**COTh**.

is highly challenging. The primary challenge lies in diastereoselective (homochiral) connection of sterically hindered precursors.

In the pioneering work by Rajca,[9] Marsella,[10,18] and Wong,[11] preinstallation of halogens into the building blocks were pivotal for chemoselectivities and couplings (Figure 3).
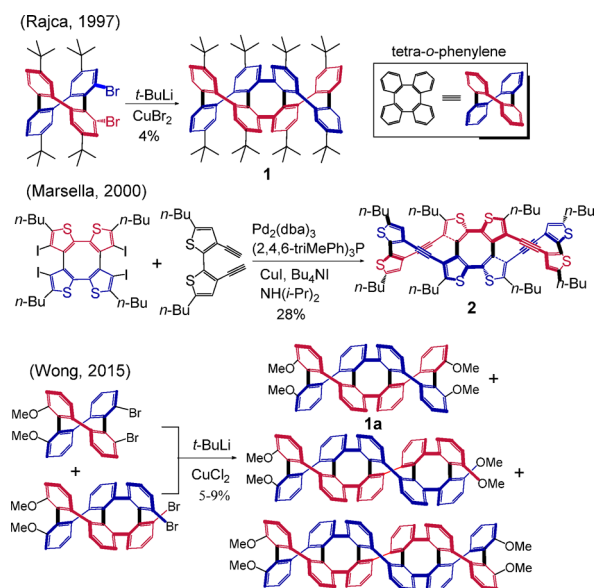
**Figure 3.** Syntheses of double helical molecules.

Rajca's tetra-o-phenylene-based double helix **1**, with four biphenyl moieties, was synthesized in 4% yield via CuBr$_2$-promoted oxidative homocoupling of a racemic tetra-o-phenylene precursor. As a continuation of Rajca's work, Wong[11] recently synthesized the optically pure homologues of octaphenylene **1** with 3, 4, 5, and 6 biphenyl moieties via the Suzuki cross-coupling reaction and the copper-mediated oxidative homocoupling reaction; in particular, starting from enantiopure tetra-o-phenylene precursor, the CuCl$_2$-mediated homocoupling gave octaphenylene **1a**, an analogue of **1**, in 16% yield. Octaphenylene **1a** and its higher homologues were obtained in low yields (5−9%) via random homocoupling of enantiopure precursors with two and three biphenyl moieties (Figure 3).[11] Marsella's conjugated double helical octathienylene **2** was obtained in 28% yield via Sonogashira cross-coupling of the saddle-shaped *racemic* α,β-**COTh** building block. The building blocks with bulky substituents and low diastereoselectivities presumably contributed to the reported

low CC-bond coupling efficiencies, starting from racemic precursors, although the introduction of the bridging acetylene units should help release the steric hindrance in the latter case.[18]

Development of convenient and efficient approaches to double helical oligomers is still highly sought, which should in turn spur the advances of this challenging field.

Our groups have been actively involved in the synthesis of oligo(thienylene) derivatives.[5,6,19,20] We discover that *rac-β,β-***COTh**-TMS$_4$ (*rac*-**3**) preferentially undergoes stepwise ipsilateral deprotonation. This prompts us to explore iterative deprotonation/coupling strategy for the synthesis of double helical molecules and oligomers, as shown in Scheme 1. In

Scheme 1. Synthetic Route to Double Helices
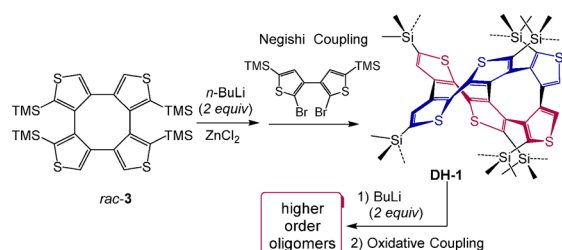
principle, these oligomers should adopt double helical geometry that is enforced by covalent C−C bond linkage. We note the two critical factors for this strategy. First, selective control of stepwise ipsilateral deprotonation of the highly strained oligomers with bulky substituents must be efficient. Second, the highly twisted racemic double helices and the thienylene building blocks should induce significant diastereoselectivity in the CC-bond forming coupling reaction.

Here we report the iterative ipsilateral deprotonation/coupling strategy to construct the double helical motifs from α,β-**COTh** and β,β-**COTh** building blocks (Schemes 1 and 4). With this synthetic strategy, we obtain racemic double helices *rac*-**DH-1**, *rac*-**DH-2** and *rac*-**DH-3** (Chart 1) in remarkable

Chart 1
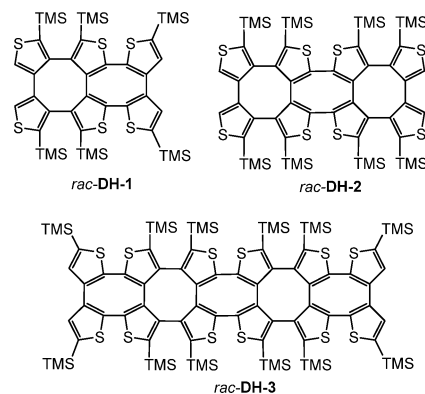
yields (26%−42%). *Rac*-**DH-3** is the longest π-conjugated thiophene-based double helix, possessing 6 bithienylene units. X-ray crystallographic studies of *rac*-**DH-1**, *rac*-**DH-2**, and *rac*-**DH-3** unambiguously reveal that each double helical scaffold has two single helices intertwined with each other via the C−C single bonds.

■ RESULTS AND DISCUSSION

Regioselective Deprotonation of β,β-COTh. We first explored the possibility of regioselective deprotonation of β,β-COTh, which is the key for successful construction of double helical motif. Although the first synthesis of β,β-COTh was reported by Kauffmann[21] in 1978, there has been no report on its regioselective deprotonation.

We first attempted to deprotonate all eight α-CH positions in β,β-COTh using 10 equiv of n-BuLi in THF at −78 °C. After the reaction mixture was warmed to 60 °C for 2 h, and quenched with TMS-Cl, to our surprise, only the product with four TMS substituents (**3**) was obtained in 73% yield (Scheme 2), rather than the anticipated octa-TMS-substituted product.

**Scheme 2. Regioselective Deprotonation of β,β-COTh**
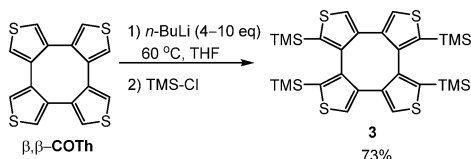
The ipsilateral substitution patterns were also notable, possibly due to lithium chelation.[22] We reason that selective deprotonation of β,β-COTh might originate in the intermediate (β,β-COTh-Li$_4$) bearing a double-bridged dilithium moieties, as suggested by Xi[23,24] in the case of 1,4-dilithio-1,3-butadiene. This might be the key factor for the observed selectivity. We then explored the loading range of n-BuLi from 4 to 10 equiv and obtained the same results. We next carefully investigated the effect of temperature. We found that the deprotonation of β,β-COTh with n-BuLi showed very low efficiency below −60 °C, but greatly improved in the temperature range of −30 to +60 °C, in which **3** was obtained in the yields of 74−80% (Table S1, SI). We also carried out reactions using s-BuLi and t-BuLi and found similar results to that of n-BuLi (Table S2, SI). Lastly, an even weaker base such as LDA provided **3** in 67% yield. When the reaction of β,β-COTh with n-BuLi was quenched with D$_2$O, 99% yield of β,β-COTh-d_4 was obtained (Table S2, SI). Therefore, we conclude that deprotonation of β,β-COTh is highly selective to give carbotetraanion/salt when >4 equiv of n-BuLi is used. The carbotetraanion/salt of β,β-COTh are quite stable over a wide temperature range, even as high as 60 °C. The structure of **3** was confirmed by X-ray crystal diffraction analysis (Figure 4).

Next, we turned our attention to the deprotonation of **3**, which has four equivalent peripheral α-CH positions. Note that regioselective formation of carbodianion/salt via ipsilateral deprotonation of **3** is the prerequisite for our synthetic

approach to double helices (Scheme 1). Treatment of **3** with 2.0 equiv n-BuLi in diethyl ether at −78 °C, then warming up to 60 °C for 2 h, and then quenching with iodine provided the expected ipsilateral diodide **4** in 70% yield (Scheme 3).

Scheme 3. Regioselective Deprotonation of rac-3
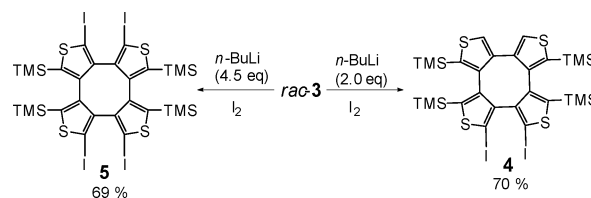
Similarly to the deprotonation of β,β-COTh, the deprotonation of **3** shows temperature dependence (Table S3, SI). The yields of **4** can reach up to 65−72% when the reaction temperature was in the 0−60 °C range. When 4.5 equiv n-BuLi was employed, a tetra-iodo substituted compound **5** was produced in 69% yield (Scheme 3). Structures of both **4** and **5** were confirmed by X-ray crystal analyses (Figure 4). We speculate that deprotonation of **3** may have occurred in a stepwise fashion, i.e., two ipsilateral deprotonations in sequence.

Syntheses of rac-DH-1, rac-DH-2 and rac-DH-3. The success in highly selective deprotonations of β,β-COTh and **3** offered us the possible synthetic pathway to novel double helical oligomers, as summarized in Scheme 4. The synthesis has three main features: (1) the precursors are racemic, (2) direct annelation of two building blocks, α,β-COTh and β,β-COTh, without any linkage, and (3) TMS groups provide protection and solubility.

The tris(bithienylene) rac-DH-1 was obtained by treatment of rac-3 with 2 equiv of n-BuLi followed by trapping with ZnCl$_2$ and subsequent Negishi coupling with 2,2′-dibromo-5,5′-di(trimethylsilyl)-3,3′-bithiophene (**6**). The overall yield was 33%. Likewise, the tetrakis(bithienylene) rac-DH-2 was readily produced by CuBr$_2$-mediated oxidative coupling of rac-3-Li$_2$ in a higher 42% yield over two steps. Further deprotonation of the rac-DH-1 at its only two α-CH positions, using 2.5 equiv of n-BuLi at 60 °C, again displays high ipsilateral selectivity, as evidenced by isolation d_2-quenching product rac-DH-1-d_2 in 99% yield. Upon treatment of rac-DH-1 with 2+ equiv of n-BuLi, followed by the addition of CuCl$_2$, resulted in oxidative dimerization of the likely rac-DH-1-Li$_2$ intermediate. As a result, a higher order homologous double helix, namely hexakis(bithienylene), rac-DH-3 was obtained in 26% yield (over 2 steps). Two side products were also identified to be DH-1 bearing two Cl groups, such as $meso$-DDH-1-Cl$_2$ and DH-1-Cl$_2$ isolated in 11% and 22% yields, respectively (Scheme
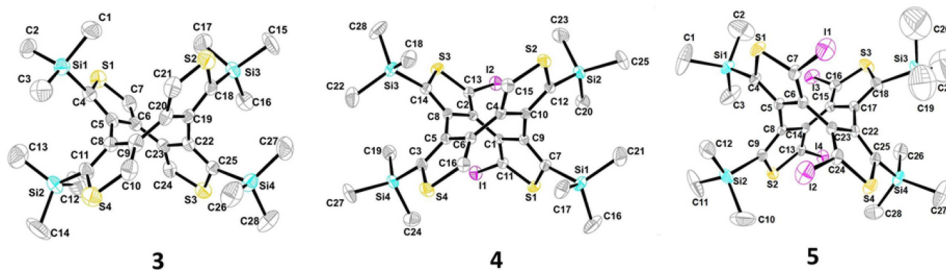
Figure 4. Crystal structures of **3**, **4**, and **5** (from left to right). Carbon, silicon, sulfur and iodine atoms are depicted with thermal ellipsoids set at the 30% probability level. All hydrogen atoms are omitted for clarity.

**Scheme 4. Synthetic Route to Racemic Double Helical Molecules**
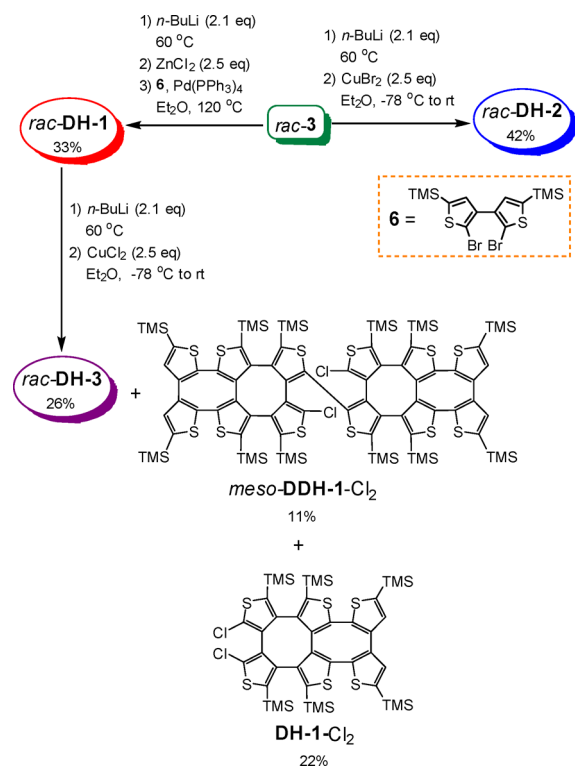
4).[9,25] NMR spectra of crude reaction mixtures for *rac*-**DH-2**, produced by CuBr$_2$-mediated oxidative coupling of *rac*-**3**-Li$_2$, indicate absence of similar bromo-substituted byproducts (Figure S24, SI). These results clearly demonstrate the efficiency of the iterative deprotonation/coupling strategy in the construction of the double helical oligomers.

As evident in preparation of COThs,[19a,21,26,27] construction of eight-membered thienylene-derived rings generally results in very low yields, presumably due to highly disfavored strain residing in the products. In comparison, the more twisted geometries in the double helical motifs should induce additional molecular strains, and consequently gives poorer yields (e.g., 4% coupling yield for making octaphenylene **1** by Rajca[9]). However, our approach to the double helical oligomers exhibits reasonably good coupling efficiency. The key attribute is the formation of highly stable lithiated carbodianions after ipsilateral deprotonation of the TMS-thienylene precursors at 60 °C. The subsequent coupling provides *rac*-**DH-1**, *rac*-**DH-2**, and *rac*-**DH-3** in 33%, 42%, and 26% yields, respectively. Very low yields of products and various side products were obtained if the deprotonation reactions were run at −78 °C, possibly due to a slow or incomplete deprotonation process. We believe that highly efficient formation of lithiated carboanions is the key for preparation of the double helical oligomers.

To date, the syntheses of chiral double helices strictly requires optically pure starting materials.[11,25,28] In the present work, we utilized a racemic mixture ((*R,R,R*)-**DH-1** and (*S,S,S*)-**DH-1**), where the (*R*)/(*S*) labels for three chiral axes pertain to the three 3,3′-bithienylene moieties, as the precursor for **DH-3**. We note that **DH-3** has six chiral axes, which means only three isomers, two enantiomers (*R,R,R,R,R,R*)-**DH-3** and (*S,S,S,S,S,S*)-**DH-3**, and a plausible *meso*-**DH-3** could be obtained from dimers **A**, **B**, and **C** (Figure 5), respectively. The dimers **A**, **B**, and **C** might be formed by coupling of (*R,R,R*)-**DH-1** and (*S,S,S*)-**DH-1**. The next ring closure coupling can occur within the dimers **A** and **B** to generate *rac*-**DH-3** in 26% yield. Meanwhile, the side-product, *meso*-**DDH-1-Cl$_2$**, was generated in 11% yield, due to the failure of the ring closure of dimer **C** (*meso* compound). The yield of *rac*-**DH-3** is about twice to that of *meso*-**DDH-1-Cl$_2$**, which implies a significant diastereoselectivity for the initial C−C bond
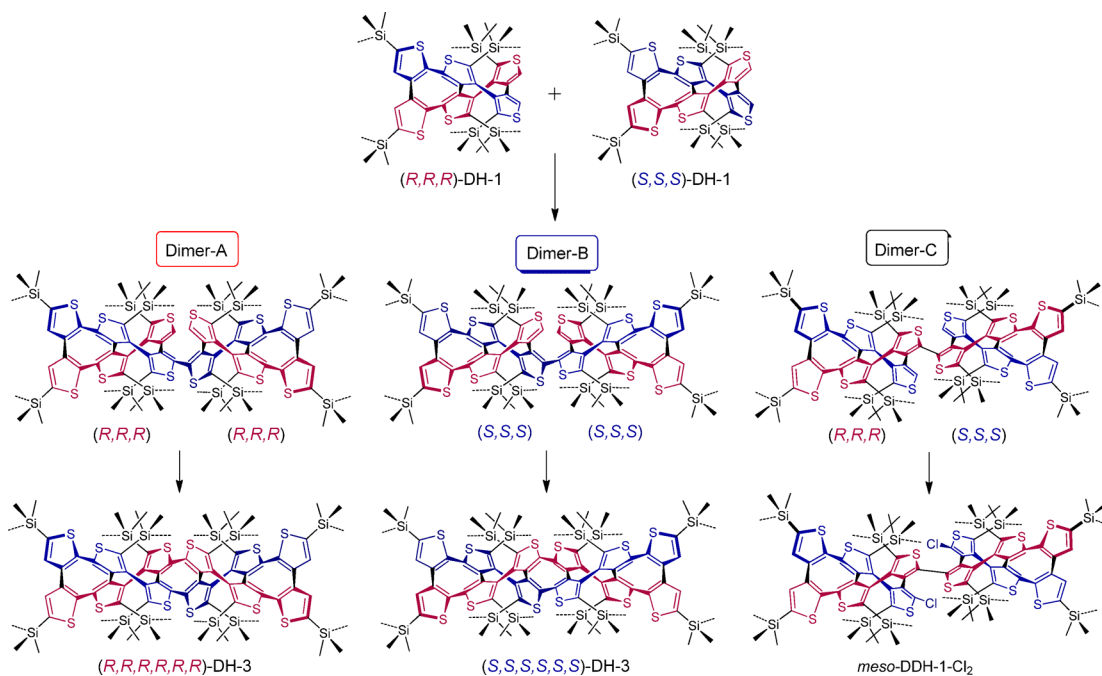
Figure 5. Possible formation of *rac*-**DH-3** from *rac*-**DH-1**. (*R*)/(*S*) labels indicate configuration of chiral axes associated with 3,3′-bithienylene moieties.
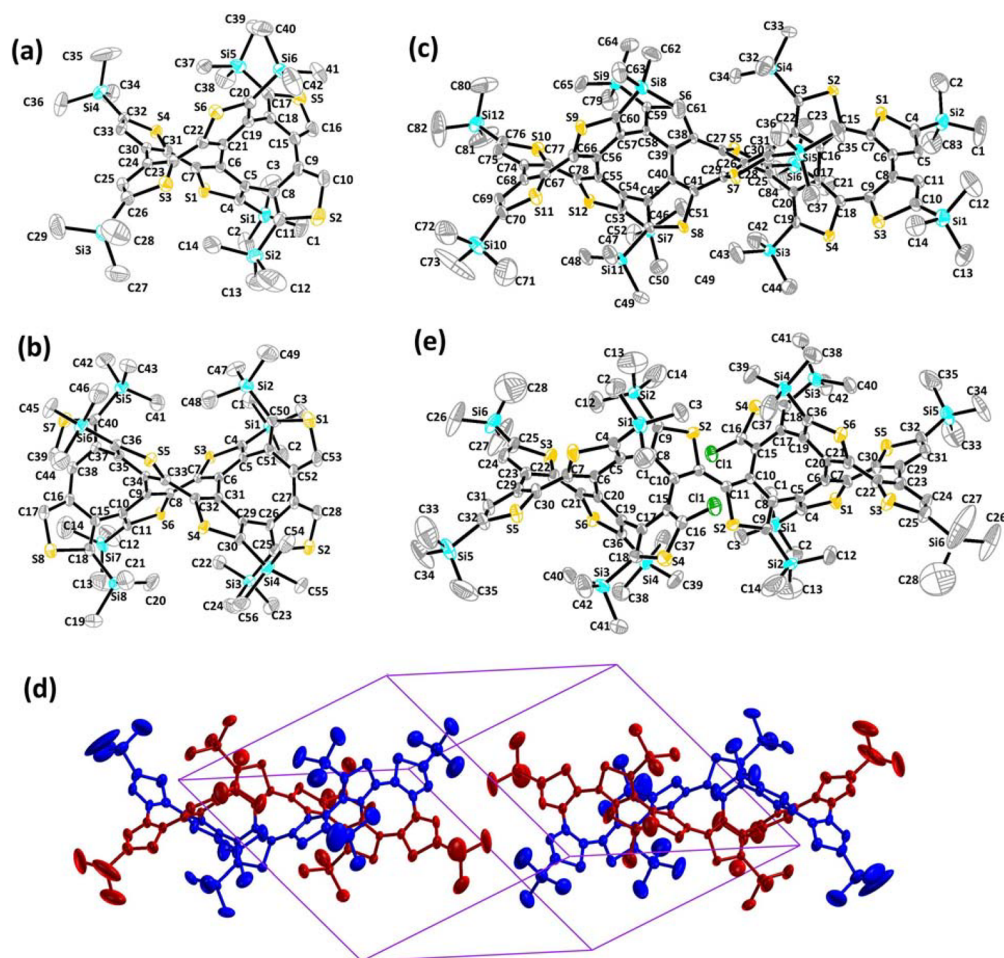
Figure 6. X-ray crystal structures of *rac*-**DH-1** (a), *rac*-**DH-2** (b), *rac*-**DH-3** (c), the crystal cell of *rac*-**DH-3** (d), and *meso*-**DDH-1**-Cl$_2$ (e) (side view). *rac*-**DH-3** (d) showing two repeat units of one supramolecular polymer chain that form across the two vertex angles of cell. Carbon, silicon, sulfur, and chlorine atoms are depicted with thermal ellipsoids set at the 30% probability level. All hydrogen atoms are omitted for clarity.

Table 1. Data for X-ray Crystal Structures[a]

compound	averaged dihedral angle (deg)					averaged inner angle (deg)				
TMS$_4$-α,β-COTh	37.7 (A)[a27]					128.4 (A)[27]				
TMS$_4$-β,β-COTh (3)	51.0 (B)[a]					121.9 (B)				
	A$_1$	B$_1$	A$_2$	B$_2$	A$_3$	A$_1$	B$_1$	A$_2$	B$_2$	A$_3$
rac-**DH-1**	42.0	51.1				126.6	121.9			
rac-**DH-2**	42.0	49.7		51.6		126.5	122.2		122.7	
rac-**DH-3**	40.7	50.1	39.0	50.3	40.6	127.1	122.3	127.7	122.2	127.2

[a]**A** corresponds to **TMS$_4$-α,β-COTh** moiety and **B** corresponds to **TMS$_4$-β,β-COTh (3)** moiety.

formation between homochiral **DH-1** building blocks leading to dimers **A** and **B**.[29]

X-ray Crystal Structure Analyses of Double Helical Oligomers. The three double helical oligomers, *rac*-**DH-1**, *rac*-**DH-2**, and *rac*-**DH-3**, as well as *meso*-**DDH-1**-Cl$_2$, can be crystallized from chloroform/methanol; they crystallize in monoclinic/space point *P*2(1)/c, monoclinic/space point *C*2/c, triclinic/space point *P*-1, and triclinic/space point *P*-1, respectively. Their crystal structures are shown in Figure 6, from which the double helical molecular structures can be visualized directly. *Rac*-**DH-1**, *rac*-**DH-2**, and *rac*-**DH-3** have two, three, and five COTh moieties, respectively. These COTh moieties are sequentially annelated together in the molecules, which contain double helical structures intertwined with each

other via the C−C single bonds. The molecular lengths extend from 7.884 Å (S2···C26) to 11.921 Å (C39···C53) and 17.956 Å (C11···C69) for *rac*-**DH-1**, *rac*-**DH-2**, and *rac*-**DH-3**, respectively. In addition, the dihedral angle of the two terminal thiophene rings of each strand (blue or red strand, Figure 5) in the double helical oligomer are measured, and the average value increased from 127° to 196° and 298° for *rac*-**DH-1**, *rac*-**DH-2**, and *rac*-**DH-3**, respectively.

In packing of *rac*-**DH-3**, two enantiomers ((*R*,*R*,*R*,*R*,*R*,*R*)-**DH-3** and (*S*,*S*,*S*,*S*,*S*,*S*)-**DH-3**) per unit cell are shown in Figure 6d. Only two H1A···H12A short interactions (2.261 Å) between the repeat two enantiomer units form one supramolecular polymer chain across the two vertex angles of cell. Similar observations were reported in the self-aggregation of

helicenes,[30] and tetra(phenylacetyl)-α,β-**COTh**.[18] In addition, another two H11B⋯H44A short interactions (2.325 Å) between two adjacent enantiomers from two neighboring supramolecular polymer chains link the polymer chains to form crystal packing pattern.

In the crystal of *meso*-**DDH-1**-Cl₂, one molecule per unit cell packing one by one is shown along the *a*-axis. Only intermolecular interaction between S1⋯H27C is observed with distance of 2.911 Å. Each molecule combines with two molecules of chloroform. The distance between two Cl1 atoms is 7.505 Å, and the distance between two C16 atoms (Figure 6e) is 7.093 Å. Such distance implies significant disfavored steric interaction for ring closure coupling to generate *meso*-**DH-3** from dimer-**C**.

More interestingly, *rac*-**DH-1**, *rac*-**DH-2**, and *rac*-**DH-3** are independently constructed by one α,β-**COTh** and one β,β-**COTh**, one α,β-**COTh** and two β,β-**COTh**, and three α,β-**COTh** and two β,β-**COTh**, respectively. The averaged dihedral angles (θ) and averaged inner angles (α) of α,β-**COTh** and β,β-**COTh** moieties bearing four TMS groups are measured to be 37.7°, 51.0° and 128.4°, 121.9° (Table 1), respectively. It is also interesting to note that all α,β-**COTh** and β,β-**COTh** moieties in the three double helical oligomers retain their parent conformations because the angles θ and α within the moieties are similar to those in α,β-**COTh** and β,β-**COTh** molecules. This suggests that little, if any, extra strain is introduced in the annelation process leading to the double helical oligomers.

Electronic Absorption Spectra of Double Helical Oligomers. UV−vis absorption spectra of α,β-**COTh** and β,β-**COTh** were used to evaluate electron delocalization in *rac*-**DH-1**, *rac*-**DH-2**, and *rac*-**DH-3** (Figure 7). β,β-**COTh** shows
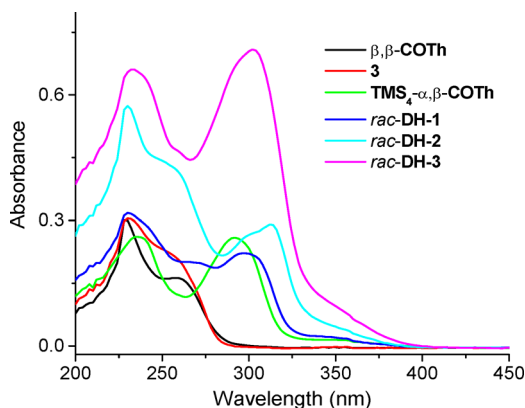
Figure 7. UV−vis absorption spectra in dichloromethane at room temperature ([C] = 1 × 10⁻⁵ M).

two peaks at 232 and 265 nm (shoulder). Meanwhile, (TMS)₄-α,β-**COTh** shows two peaks at 234 and 290 nm and a weak band at ∼350 nm. Double helices *rac*-**DH-1**, *rac*-**DH-2**, and *rac*-**DH-3** show four absorption bands at ∼230 nm, ∼265 nm (shoulder), ∼300 nm, and a very weak band at ∼350 nm (shoulder). Besides the significant increases in absorbance, peaks at ∼230 nm remain at the same wavelength, while the other bands show small bathochromic shifts with increasing length of the double helix. We rationalize this behavior by noting that α,β-**COTh** and β,β-**COTh** moieties are sequentially annelated in the double helical oligomers, forming cross-conjugated π-system of 2,2′-bithienyls, which shows significant increases in absorbance but weak bathochromic shifts. This

behavior is analogous to that observed in cross-conjugated carbon−sulfur [n]helicenes (Figure 1).[5,28,31]

Resolution of Double Helix DH-1-D: Barrier for Racemization and Chirooptical Properties. For resolution of double helical oligomers, we chose chiral AD-H column, which gave baseline resolution of enantiomers in racemic carbon−sulfur [n]helicenes (n = 7, 9, and 11).[5d,e,28,31] Thus, we were disappointed to find out that the chromatograms for *rac*-**DH-1**, *rac*-**DH-2**, and *rac*-**DH-3** showed only a single sharp peak (Figures S1−S3, SI). Therefore, we removed TMS groups using trifluoroacetic acid to obtain cleanly the corresponding deprotected double helices *rac*-**DH-1-D**, *rac*-**DH-2-D**, and *rac*-**DH-3-D**. However, only *rac*-**DH-1-D** had sufficient solubility in organic solvents to permit resolution with chiral HPLC;[32] we obtained a fraction of mg of (+)-**DH-1-D** and (−)-**DH-1-D** with 99+% enantiomeric excess (ee) (Figure S1, SI).

Since pure enantiomers had a melting point of 294 °C, we attempted racemization of (+)-enantiomer at 298 °C on air using melting point capillaries and following the progress of the reaction by chiral HPLC. However, even after heating at 298 °C for 120 min, the chromatograms of these samples show only one peak, with a broad shoulder near the baseline (Figure S4, SI). Thus, assuming that up to 5% of (−)-enantiomer has formed, we estimate the lower limit for the barrier for racemization as $\Delta G^{\ddagger} > 48$ kcal mol⁻¹. This barrier is significantly higher than the barrier $\Delta G^{\ddagger} = 43.5$ kcal mol⁻¹ for racemization of [9]helicene[33] but most likely lower than B3LYP and MP2-computed barrier of about 79 kcal mol⁻¹ for ring inversion in tetra-*o*-phenylene.[34,35]

Enantiomers of double helix **DH-1-D** possess moderate optical rotations, e.g., for (−)-enantiomer, $[\alpha]_D \approx -176$ (c 0.036, cyclohexane) 10⁻¹ deg cm² g⁻¹,[36a,b] which is significantly weaker than $[\alpha]_D = -1019 \times 10^{-1}$ deg cm² g⁻¹ for carbon−sulfur [7]helicene. CD spectra show helicene-like spectral pattern with the sign of the longest wavelength Cotton effect corresponding to the sign of $[\alpha]_D$; that is, the sign is negative for the (−)-enantiomer with $\Delta\varepsilon_{max} \approx -11.0$ L mol⁻¹ cm⁻¹ at 327 nm (Figure 8).[36b,c]

The strength of chiroptical properties in absorption may be measured by the corresponding anisotropy factors (g-values).[37,38] Thus, for (−)-**DH-1-D**, $g = \Delta\varepsilon/\varepsilon = -0.039$, based on $\Delta\varepsilon_{max} = -11.0$ and $\varepsilon = 2.8 \times 10^2$ L mol⁻¹ cm⁻¹ at 327 nm in cyclohexane, may be compared to $g = \Delta\varepsilon/\varepsilon = -4 \times 10^{-3}$ for carbon−sulfur [7]helicene, in which $\Delta\varepsilon_{max} = -117$ and $\varepsilon = 3.1 \times 10^4$ L mol⁻¹ cm⁻¹ at 285 nm.[28,38] This implies significantly stronger chiroptical properties for the double helix (−)-**DH-1-D** than for carbon−sulfur [7]helicene.

High barrier for racemization and the significant strength of chiroptical properties in **DH-1-D** indicate thiophene-based double helical oligomers with their unique structures have a potential to become a significant player in the field of chiral materials, analogously to tetraphenylenes.[12,39] Moreover, thiophene-based double helices may provide a new chiral molecular architecture for the emerging field of chiral organic conducting systems.[40]

DFT Modeling of Barrier for Racemization and CD Spectra for DH-1-D. All geometries were optimized at the B3LYP/6-31G(d,p)+ZPVE level of theory; transition states were characterized by intrinsic reaction coordinate (IRC) computations.[41]

As expected, global minimum structures for α,β-**COTh**, β,β-**COTh** and **DH-1-D** possess D₂, D₂d, and C₂ point groups of symmetry, respectively (Table 2). The planar structures of α,β-
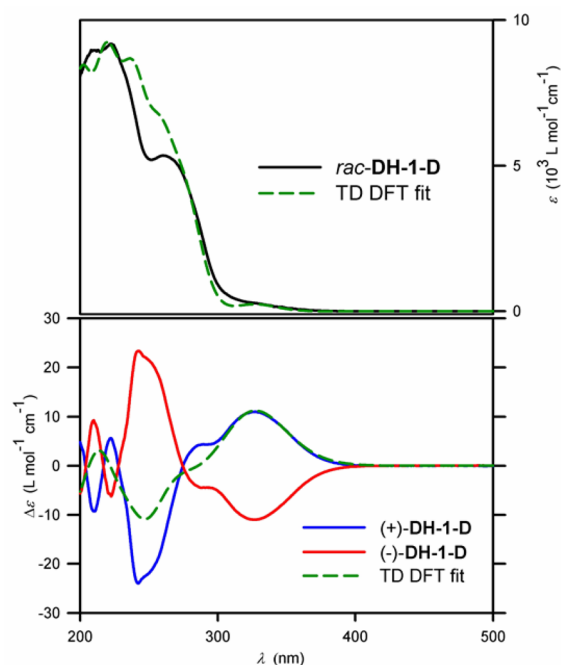
Figure 8. UV−vis absorption spectra and CD spectra for **DH-1-D** in cyclohexane (solid lines).[36c] TD DFT-computed spectra at the CAM-B3LYP/6-31+G(d,p)/IEF-PCM-UFF (cyclohexane) level of theory. Both computed spectra were shifted by −0.15 eV and scaled vertically.

Table 2. Barriers for Ring Inversion (racemization) in Tetrathienylenes and in Double Helix DH-1-D at the B3LYP/6-31G(d,p)+ZPVE Level of Theory

Compound	Point group of symmetry (number of imaginary frequencies)	Critical point	Relative energy (kcal mol⁻¹)
α,β-**COTh**	D_2 (0)	minimum	**0.00**
α,β-**COTh**	C_i (1)	TS	29.51
α,β-**COTh**	D_{2h} (3)		29.77
β,β-**COTh**	D_{2d} (0)	minimum	**0.00**
β,β-**COTh**	D_4 (1)	TS	45.24
β,β-**COTh**	D_{4h} (4)		47.09
DH-1-D	C_2 (0)	minimum	**0.00**
DH-1-D	C_2 (0)	minimum	39.52
DH-1-D	C_2 (1)	TS	42.75
DH-1-D	C_1 (1)	TS	**51.03**
DH-1-D	C_{2v} (7)		138.03

COTh, β,β-**COTh** and **DH-1-D**, with D_{2h}-, D_{4h}-, and C_{2v}-symmetries, are at 29.77, 47.09, and 138.03 kcal mol⁻¹ above their corresponding global minimum structures and correspond to the critical points with multiple imaginary frequencies. The transition states (one imaginary frequency) for ring flip in α,β-**COTh** and β,β-**COTh**, with C_i and D_4 point groups of symmetry, are at 29.51 and 45.24 kcal mol⁻¹ above their corresponding global minimum structures, that is, only slightly below the planar structures.

For **DH-1-D**, two transition states were identified at 42.75 and 51.03 kcal mol⁻¹ above the global minimum. The C_2-symmetric global minimum structure may be viewed as possessing three 3,3′-bithienylene moieties associated with the three chiral axes of the same configuration. IRC computations revealed that both transition states are connected to the global minimum on one side and to the second C_2-symmetric minimum on the other side, which is 39.52 kcal mol⁻¹ higher in energy. The second minimum structure possesses two terminal 3,3′-bithienylene moieties with opposite configurations and the center 3,3′-bithienylene moiety is flattened. The process of racemization of **DH-1-D** is complex because it involves inversion of the chiral axes associated with three 3,3′-bithienylene moieties (Figure 9). This process of
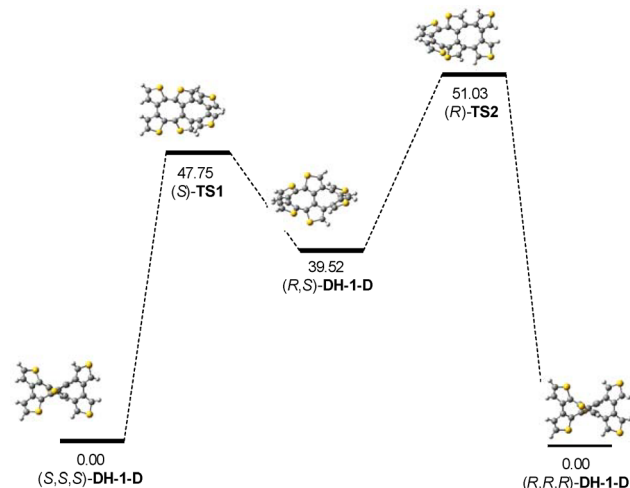
Figure 9. Potential energy surface for racemization of **DH-1-D** at the B3LYP/6-31G(d,p)+ZPVE level of theory.

racemization may be thought as involving two chiral axes at the same time. First, the two 3,3′-bithienylene moieties flatten, forming the lower energy transition state with nearly planar α,β-**COTh** moiety. Second, the terminal 3,3′-bithienylene moiety within α,β-**COTh** moiety acquires inverted configuration forming the second minimum structure, and then next the other terminal 3,3′-bithienylene moiety flattens, forming the highest energy transition state with nearly planar β,β-**COTh** moiety. Finally, the two 3,3′-bithienylene moieties within nearly planar β,β-**COTh** moiety invert their configuration, thus forming enantiomer of **DH-1-D**.

Theoretical modeling of the UV−vis absorption and CD spectra was carried out at the CAM-B3LYP/6-31+G(d,p) level in IEF-PCM-UFF-modeled cyclohexane and using B3LYP/6-31G(d,p)-optimized geometries.[41] Both computed spectra were shifted by −0.15 eV and scaled vertically to obtain reasonable fit to the experimental data (Figure 8).

■ CONCLUSIONS

We demonstrate a facile and efficient "iterative deprotonation/CC-bond coupling" strategy for the construction of a conjugated double helical ladder oligomers, starting from the achiral, saddle-shaped β,β-**COTh** building block. The highly regioselective deprotonation of β,β-**COTh**, using *n*-BuLi, is the key step in the synthetic strategy. Diastereoselectivity is crucial for the formation of double helices *rac*-**DH-2** and *rac*-**DH-3** from racemic precursors (*rac*-**3** and *rac*-**DH-1**), in which *rac*-

DH-3 showcases the longest double helix. These distinctive features provide a possibility to establish a general guideline for preparation of double helical oligomers with a defined length. Furthermore, the X-ray crystallographic studies on the three double helical oligomers clearly show the molecular structures of π-conjugated double helical ladder oligomers. Resolution of *rac*-**DH-1-D** allowed us to establish both strong chirooptical properties and large barriers for racemization of the lowest double helical homologue. Although the resolution of the higher homologues was not successful, this work will facilitate the synthetic approaches to enantiopure double helical ladder oligomers and provide a configurationally stable framework for the construction of organic materials based upon chiral π-conjugated systems.

ASSOCIATED CONTENT

ⓢ Supporting Information

The Supporting Information is available free of charge on the ACS Publications website at DOI: 10.1021/jacs.6b05709.

> Crystal data in CIF and DFT computational results for the corresponding products (CIF)
>
> Crystal data in CIF and DFT computational results for the corresponding products (CIF)
>
> Crystal data in CIF and DFT computational results for the corresponding products (CIF)
>
> Crystal data in CIF and DFT computational results for the corresponding products (CIF)
>
> Crystal data in CIF and DFT computational results for the corresponding products (CIF)
>
> Crystal data in CIF and DFT computational results for the corresponding products (CIF)
>
> Crystal data in CIF and DFT computational results for the corresponding products (CIF)
>
> Complete ref 41, general experimental procedures, synthesis, spectroscopic data (^{1}H NMR, ^{13}C NMR, and HRMS), and chiral HPLC chromatograms (PDF)

AUTHOR INFORMATION

Corresponding Authors

*songjs@henu.edu.cn

*arajca1@unl.edu

*hwang@henu.edu.cn

Notes

The authors declare no competing financial interest.

ACKNOWLEDGMENTS

REFERENCES

(1) (a) Cinar, M. E.; Ozturk, T. *Chem. Rev.* **2015**, *115*, 3036−3140. (b) Mishra, A.; Ma, C.-Q.; Bäuerle, P. *Chem. Rev.* **2009**, *109*, 1141−1276. (c) Miller, L. L.; Mann, K. R. *Acc. Chem. Res.* **1996**, *29*, 417−423. (d) Bäuerle, P.; Segelbacher, U.; Maier, A.; Mehring, M. *J. Am. Chem. Soc.* **1993**, *115*, 10217−10223.

(2) (a) Facchetti, A.; Deng, Y.; Wang, A.; Koide, Y.; Sirringhaus, H.; Marks, T. J.; Friend, R. H. *Angew. Chem., Int. Ed.* **2000**, *39*, 4547−4551. (b) Schoonveld, W. A.; Wildeman, J.; Fichou, D.; Bobbert, P. A.; van Wees, B. J.; Klapwijk, T. M. *Nature* **2000**, *404*, 977−980. (c) Cnops, K.; Rand, B. P.; Cheyns, D.; Verreet, B.; Empl, M. A.; Heremans, P. *Nat. Commun.* **2014**, *5*, 4406.

(3) (a) Xiao, K.; Liu, Y.; Qi, T.; Zhang, W.; Wang, F.; Gao, J.; Qiu, W.; Ma, Y.; Cui, G.; Chen, S.; Zhan, X.; Yu, G.; Qin, J.; Hu, W.; Zhu, D. *J. Am. Chem. Soc.* **2005**, *127*, 13281−13286. (b) Zhang, X.; Côté, A. P.; Matzger, A. J. *J. Am. Chem. Soc.* **2005**, *127*, 10502−10503. (c) Kim, E.; Coropceanu, V.; Gruhn, N. E.; Sánchez-Carrera, R. S.; Snoeberger, R.; Matzger, A. J.; Brédas, J. *J. Am. Chem. Soc.* **2007**, *129*, 13072−13081.

(4) (a) Chernichenko, K. Y.; Sumerin, V. V.; Shpanchenko, R. V.; Balenkova, E. S.; Nenajdenko, V. G. *Angew. Chem., Int. Ed.* **2006**, *45*, 1−4. (b) Dadvand, A.; Cicoira, F.; Chernichenko, K. Y.; Balenkova, E. S.; Osuna, R. M.; Rosei, F.; Nenajdenko, V. G.; Perepichka, D. F. *Chem. Commun.* **2008**, 5354−5356. (c) Ivasenko, O.; MacLeod, J. M.; Chernichenko, K. Y.; Balenkova, E. S.; Shpanchenko, R. V.; Nenajdenko, V. G.; Rosei, F.; Perepichka, D. F. *Chem. Commun.* **2009**, 1192−1194.

(5) (a) Rajca, A.; Wang, H.; Pink, M.; Rajca, S. *Angew. Chem., Int. Ed.* **2000**, *39*, 4481−4483. (b) Torroba, T.; García-Valverde, M. *Angew. Chem., Int. Ed.* **2006**, *45*, 8092−8096. (c) Zak, J. K.; Miyasaka, M.; Rajca, S.; Lapkowski, M.; Rajca, A. *J. Am. Chem. Soc.* **2010**, *132*, 3246−3247. (d) Miyasaka, M.; Pink, M.; Rajca, S.; Rajca, A. *Angew. Chem., Int. Ed.* **2009**, *48*, 5954−5957. (e) Miyasaka, M.; Rajca, A.; Pink, M.; Rajca, S. *J. Am. Chem. Soc.* **2005**, *127*, 13806−13807.

(6) (a) Li, C.; Shi, J.; Xu, L.; Wang, Y.; Cheng, Y.; Wang, H. *J. Org. Chem.* **2009**, *74*, 408−411. (b) Wang, Z.; Shi, J.; Wang, J.; Li, C.; Tian, X.; Cheng, Y.; Wang, H. *Org. Lett.* **2010**, *12*, 456−459. (c) Liu, X.; Yu, P.; Xu, L.; Yang, J.; Shi, J.; Wang, Z.; Cheng, Y.; Wang, H. *J. Org. Chem.* **2013**, *78*, 6316−6321. (d) Li, L.; Zhao, C.; Wang, H. *Chem. Rec.* **2016**, *16*, 797−809.

(7) (a) Korevaar, P. A.; de Greef, T. F. A.; Meijer, E. W. *Chem. Mater.* **2014**, *26*, 576−586. (b) Schlütter, F.; Nishiuchi, T.; Enkelmann, V.; Müllen, K. *Angew. Chem., Int. Ed.* **2014**, *53*, 1538−1542. (c) Khalil, G. E.; Adawi, A. M.; Robinson, B.; Cadby, A. J.; Tsoi, W. C.; Kim, J.-S.; Charas, A.; Morgado, J.; Lidzey, D. G. *J. Phys. Chem. B* **2011**, *115*, 12028−12035. (d) Tian, Y.; Park, G.; Kertesz, M. *Chem. Mater.* **2008**, *20*, 3266−3277. (e) Anthony, J. E. *Chem. Rev.* **2006**, *106*, 5028−5048.

(8) (a) Luh, T.-Y. *Acc. Chem. Res.* **2013**, *46*, 378−389. (b) Sakai, N.; Matile, S. *J. Am. Chem. Soc.* **2011**, *133*, 18542−18545. (c) Lin, N.-T.; Lin, S.-Y.; Lee, S.-L.; Chen, C.-H.; Hsu, C.-H.; Hwang, L. P.; Xie, Z.-Y.; Chen, C.-H.; Huang, S.-L.; Luh, T.-Y. *Angew. Chem., Int. Ed.* **2007**, *46*, 4481−4485.

(9) Rajca, A.; Safronov, A.; Rajca, S.; Shoemaker, R. *Angew. Chem., Int. Ed. Engl.* **1997**, *36*, 488−491.

(10) Marsella, M. J. *Acc. Chem. Res.* **2002**, *35*, 944−951.

(11) Chen, J. X.; Han, J. W.; Wong, H. N. C. *Org. Lett.* **2015**, *17*, 4296−4299.

(12) (a) Han, J.-W.; Li, X.; Wong, H. N. C. *Chem. Rec.* **2015**, *15*, 107−131. (b) Huang, H.; Hau, C.-K.; Law, C. C. M.; Wong, H. N. C. *Org. Biomol. Chem.* **2009**, *7*, 1249−1257. (c) Rajca, A.; Rajca, S.; Pink, M.; Miyasaka, M. *Synlett* **2007**, *2007*, 1799−1822.

(13) (a) Lehn, J.-M.; Rigault, A. *Angew. Chem., Int. Ed. Engl.* **1988**, *27*, 1095−1097. (b) Koert, U.; Harding, M. M.; Lehn, J. M. *Nature* **1990**, *346*, 339−342. (c) Hasenknopf, B.; Lehn, J. M.; Baum, G.; Fenske, D. *Proc. Natl. Acad. Sci. U. S. A.* **1996**, *93*, 1397−1400.

(14) Huc, I.; Lehn, J.-M.; Berl, V.; Khoury, R. G.; Krische, M. J. *Nature* **2000**, *407*, 720−723.

(15) Berl, V.; Huc, I.; Khoury, R. G.; Lehn, J.-M. *Chem. - Eur. J.* **2001**, *7*, 2810−2820.

(16) Watson, J. D.; Crick, F. H. C. *Nature* **1953**, *171*, 737−738.

(17) (a) Tanaka, Y.; Katagiri, H.; Furusho, Y.; Yashima, E. *Angew. Chem., Int. Ed.* **2005**, *44*, 3867−3870. (b) Ikeda, M.; Tanaka, Y.; Hasegawa, T.; Furusho, Y.; Yashima, E. *J. Am. Chem. Soc.* **2006**, *128*, 6806−6807. (c) Maeda, T.; Furusho, Y.; Sakurai, S.; Kumaki, J.; Okoshi, K.; Yashima, E. *J. Am. Chem. Soc.* **2008**, *130*, 7938−7945.

(18) Marsella, M. J.; Kim, I. T.; Tham, F. *J. Am. Chem. Soc.* **2000**, *122*, 974−975.

(19) (a) Wang, Y.; Song, J.; Xu, L.; Kan, Y.; Shi, J.; Wang, H. *J. Org. Chem.* **2014**, *79*, 2255−2262. (b) Wang, Y.; Gao, D.; Shi, J.; Kan, Y.; Song, J.; Li, C.; Wang, H. *Tetrahedron* **2014**, *70*, 631−636. (c) Sun, H.; Shi, J.; Zhang, Z.; Zhang, S.; Liang, Z.; Wan, S.; Cheng, Y.; Wang, H. *J. Org. Chem.* **2013**, *78*, 6271−6275. (d) Wu, T.; Shi, J.; Li, C.; Song, J.; Xu, L.; Wang, H. *Org. Lett.* **2013**, *15*, 354−357.

(20) (a) Xiao, S.; Pink, M.; Wang, H.; Rajca, S.; Rajca, A. *J. Sulfur Chem.* **2008**, *29*, 425−432. (b) Miyasaka, M.; Pink, M.; Rajca, S.; Rajca, A. *Org. Lett.* **2010**, *12*, 3230−3233. (c) Swager, T. M.; Batson, J. *Synfacts* **2010**, *2010*, 1136−1136.

(21) Kauffmann, T.; Greving, B.; Kriegesmann, R.; Mitschker, A.; Woltermann, A. *Chem. Ber.* **1978**, *111*, 1330−1336.

(22) Streitwieser, A., Jr. *Acc. Chem. Res.* **1984**, *17*, 353−357.

(23) (a) Xi, Z. *Acc. Chem. Res.* **2010**, *43*, 1342−1351. (b) Liu, L.; Zhang, W.; Luo, Q.; Li, H.; Xi, Z. *Organometallics* **2010**, *29*, 278−281.

(24) Wang, C.; Luo, Q.; Sun, H.; Guo, X.; Xi, Z. *J. Am. Chem. Soc.* **2007**, *129*, 3094−3095.

(25) Rajca, A.; Safronov, A.; Rajca, S.; Wongsriratanakul, J. *J. Am. Chem. Soc.* **2000**, *122*, 3351−3357.

(26) Kabir, S. M. H.; Miura, M.; Sasaki, S.; Harada, G.; Kuwatani, Y.; Yoshida, M.; Iyoda, M. *Heterocycles* **2000**, *52*, 761−774.

(27) Wang, Y.; Wang, Z.; Zhao, D.; Wang, Z.; Cheng, Y.; Wang, H. *Synlett* **2007**, *2007*, 2390−2394.

(28) Rajca, A.; Miyasaka, M.; Pink, M.; Wang, H.; Rajca, S. *J. Am. Chem. Soc.* **2004**, *126*, 15211−15222.

(29) Analysis of crude NMR spectrum also reveals that the yield of *rac*-**DH-3** is about twice to that of *meso*-**DDH-1**-Cl₂ (Figure S29, SI).

(30) Lovinger, A. J.; Nuckolls, C.; Katz, T. J. *J. Am. Chem. Soc.* **1998**, *120*, 264−268.

(31) (a) Miyasaka, M.; Pink, M.; Rajca, A.; Rajca, S. *Chem. - Eur. J.* **2004**, *10*, 6531−6539. (b) Miyasaka, M.; Pink, M.; Olankitwanit, A.; Rajca, S.; Rajca, A. *Org. Lett.* **2012**, *14*, 3076−3079. (c) Swager, T. M.; Gutierrez, G. D. *Synfacts* **2012**, *8*, 0964.

(32) *rac*-**DH-1**-**D** was resolved using analytical scale ChiralPak AD-H column with *n*-hexane/isopropanol (90:10, v/v) as eluent and flow rate of 1.0 mL/min.

(33) Martin, R. H.; Marchant, M. J. *Tetrahedron* **1974**, *30*, 347−349.

(34) Bachrach, S. M. *J. Org. Chem.* **2009**, *74*, 3609−3611.

(35) Huang, H.; Stewart, T.; Gutmann, M.; Ohhara, T.; Niimura, N.; Li, Y.-X.; Wen, J.-F.; Bau, R.; Wong, H. N. C. *J. Org. Chem.* **2009**, *74*, 359−369.

(36) (a) For (+)-**DH-1**-**D**, $[\alpha]_D \gg + 176$ (*c* 0.061, cyclohexane) 10^{-1} deg cm² g⁻¹. (b) Concentrations of samples used for optical rotation and CD spectra were determined using molar extinction coefficient, obtained from linear Lambert-Beer plot for *rac*-**DH-1**-**D** in cyclohexane (Figure S5, SI). (c) CD spectra for **DH-1**-**D** in cyclohexane, l_{max}/nm (De$_{max}$/L mol⁻¹ cm⁻¹): (−)-enantiomer, 327 (−11.0), 242 (+23.4); (+)-enantiomer, 327 (+11.0), 242 (−24.0).

(37) Eliel, E. L.; Wilen, S. H. *Stereochemistry of Organic Compounds*; Wiley: New York, 1994; pp 1013−1019.

(38) Rajca, A.; Miyasaka, M. In *Functional Organic Materials - Syntheses and Strategies*; Mueller, T. J. J., Bunz, U. H. F., Eds.; Wiley-VCH: New York, 2007; pp 543−577.

(39) (a) Lin, F.; Peng, H.-Y.; Chen, J.-X.; Chik, D. T. W.; Cai, Z.-W.; Yam, V. W. W.; Wong, H. N. C. *J. Am. Chem. Soc.* **2010**, *132*, 16383−16392. (b) Rajca, A.; Rajca, S. *Angew. Chem., Int. Ed.* **2010**, *49*, 672−674. (c) Shibata, T.; Chiba, T.; Hirashima, H.; Ueno, Y.; Endo, K. *Angew. Chem., Int. Ed.* **2009**, *48*, 8066−8069. (d) Peng, H.-Y.; Lam, C.-K.; Mak, T. C. W.; Cai, Z.-W.; Ma, W.-T.; Li, Y.-X.; Wong, H. N. C. *J. Am. Chem. Soc.* **2005**, *127*, 9603−9611. (e) Rajca, A.; Wang, H.; Bolshov, P.; Rajca, S. *Tetrahedron* **2001**, *57*, 3725−3735.

(40) (a) Pop, F.; Auban-Senzier, P.; Canadell, E.; Rikken, G. L. J. A.; Avarvari, N. *Nat. Commun.* **2014**, *5*, 3757. (b) Pospíšil, L.; Bednárová, L.; Štěpánek, P.; Slavíček, P.; Vávra, J.; Hromadová, M.; Dlouhá, H.; Tarábek, J.; Teplý, F. *J. Am. Chem. Soc.* **2014**, *136*, 10826−10829. (c) Pop, F.; Auban-Senzier, P.; Frackowiak, A.; Ptaszynski, K.; Olejniczak, I.; Wallis, J. D.; Canadell, E.; Avarvari, N. *J. Am. Chem.*

Soc. **2013**, *135*, 17176−17186. (d) Avarvari, N.; Wallis, J. D. *J. Mater. Chem.* **2009**, *19*, 4061−4076.

(41) Frisch, M. J.; et al. *Gaussian 09*, revision A.01; Gaussian, Inc.: Wallingford, CT, 2009.